Local Magnetic Actuation Based Laparoscopic Camera for Minimally Invasive Surgery

Hang Gu*, Meshak Bain*, Chang Jin Yen*, Sixu Fang*, Florence Leong*, Alireza Mohammadi*, Pietro Valdastri†, Denny Oetomo*

*The University of Melbourne, Australia, alirezam@unimelb.edu.au

† Vanderbilt University, USA, pietro.valdastri@vanderbilt.edu

Abstract

This paper proposes a novel Local Magnetic Actuation (LMA) based Laparoscopic Camera (LMALC) device attached to a cable-driven continuum arm for high dexterity and wide angle of vision. The main motivation of this magnetic-based camera design is to provide the camera the full mobility across all abdominal quadrants upon insertion through a laparoscopic incision. The magnetic coupling concept, implemented in the LMALC permanent magnet anchoring and actuation units, allows the camera to be completely detached from the external power unit and conveniently placed away from the incision point for better view triangulation, without taking up incision port space. In this study, the kinematic analysis of the magnetic-based cable-driven manipulator is presented, relating the pose of the continuum arm and wires displacement to the actuator revolutions driven by the external magnetic field. Experiments performed on the developed LMALC prototype platform with respect to varying inter-magnetic distance show consistency and feasibility, closely simulating the theoretical model.

1 Introduction

Surgical techniques have advanced significantly to achieve the aim of minimising surgical trauma to the patients. The introduction of a new surgical spectrum, with the minimally invasive surgery (MIS), demonstrated a major advancement from the open surgical techniques. With only multiple small incisions ranging from 0.5mm to 12mm around the abdomen [Leung et. al., 2000], the MIS approach has widely substituted the open surgery method since the 1990s [Johnson, 1997], offering great patient benefits over open surgery with lesser postoperative pain and blood loss, better cosmesis and faster recovery rate [Carbajo et. al., 1999].

Nonetheless, having only small incisions for tool incisions, the manipulation of conventional rigid surgical laparoscopic tools is severely constrained by the fulcrum of the incision point and restricted to a limited workspace in the abdominal cavity [Lai et. al., 2000]. In addition, surgeons suffer loss of triangulation, tool collisions, confined view angles and inconvenient tool operation during surgical procedures. Many researchers investigate various means to remove the rigid linkage of the laparoscopic surgical tools to provide the surgical tools complete deployment and manoeuvrability inside the abdominal cavity. The implementation of magnetic coupling eliminates the need for the surgical instruments to be connected to the external actuation units through a rigid body linkages, thus allowing mobility and dexterity of the instruments around various quadrants of the abdomen.

Magnetic coupling has been popularly employed to provide positioning, guidance and anchoring of surgical instruments away from the incision point, pioneered by Cadeddu and his team [Park et. al., 2007] with the introduction of the Magnetic Anchoring and Guidance Systems (MAGS). The investigation of MAGS started with its implementation in simple MAGS cameras [Park et. al., 2007] and surgical manipulators [Zeltser et. al., 2007], [Cadeddu et. al., 2009], using an external permanent magnet (PM) to guide and anchor surgical tools embedded with an internal PM intraabdominally. To extend the dexterity of surgical instruments intra-abdominally. preliminary research targeted on camera systems as simple instrument platforms incorporating onboard conventional actuator, i.e. DC micromotors [Hu et. al., 2009], [Terry et. al., 20012]. These cameras are driven by the internal on board micromotor to provide additional degrees of freedom (DOFs), i.e. pan, and tilt motions. Surgical retractors embedded with micromotors for actuation were also reported [Oleynikov, 2008].

The idea of actuating MAGS surgical instruments led some researchers into manipulating magnetic field interaction with the internal PM to drive the DOFs of the surgical tools. This created the term, the Local Magnetic Actuation (LMA) system. A four DOF cable-driven surgical retractor was developed by Di Natali et. al. [Di Natali et. al., 2013], utilising external PMs to transmit rotational motions to internal PM rotors for tool dexterity and manipulation. Simi et. al. [Simi et.

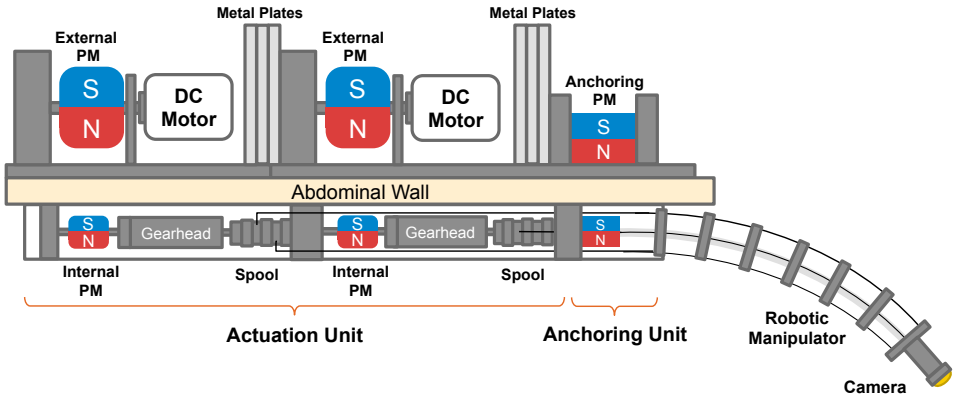

Figure 1: Schematic diagram of the LMA-based laparoscopic camera

al., 2013] proposed a LESS camera system with its position controlled by the rotational motion generated by an external magnetic field. An on board DC micromotor is used for further fine tuning of its vision angle.

In this paper, a novel LMA-based laparoscopic camera device is presented. The two DOF camera device is integrated with a cable-driven manipulator for high dexterity to achieve wide vision angle across the workspace in the abdominal cavity, thus eliminating the need in having onboard actuation for positioning. This allows the camera device to be completely independent of any actuation unit, driven only by the transmitted actuation forces and torques. Attached to an internal PM, the camera device has the capability to be anchored at any quadrant in the abdomen, while the PM rotors are coupled to the respective external PMs for actuation. The kinematic analysis of the magnetic-based cable-drive manipulator is presented and a prototype of the system is developed for experimental demonstrations and verifications.

2 LMA-based Laparoscopic Camera Mechanism

The schematic digram of the proposed LMA-based laparoscopic camera (LMALC) is shown in Fig. 1. The LMALC consists of the LMA system and a robotic manipulator which are explained in the following subsections.

2.1 Local Magnetic Actuation (LMA)

LMA implements the principle of magnetic coupling and magnetic spur gear to drive the instruments intra-abdominally [Di Natali et. al., 2015]. The LMA is composed of an anchoring unit to support the camera system during surgery and an actuation unit to transfer power to internal permanent magnet (PM) via rotating external PMs, which in turn actuates the DoFs of the robotic manipulator.

The anchoring and actuation units of the proposed LMALC are illustrated in Fig. 1. Upon deployment into the abdominal cavity through the incision point, the LMALC is guided to a desired position and anchored onto the interior abdominal wall with the anchoring magnet. The internal PMs are driven by the transmitted forces and torques generated by the externally actuated external PMs. The internal PMs then rotate the spools which wind and unwind the cables attached to the end-tip of the robotic manipulator to produce the required dexterity for camera position and vision. The camera is attached to the end tip of the robotic manipulator, tethered with a fine cable to the external power unit through the incision point.

The anchoring and actuation units are stacked in series to minimise dimension of the LMALC design and for convenient deployment. However, due to the strong magnetic attraction between the PMs, metal plates are placed between the magnets for magnetic isolation and minimisation of magnetic field interference. Although the PM provides strong magnetic coupling, it is nonetheless a fixed variable with fixed amount of magnetic field transmitting torques and forces onto the internal PM rotors. There is no variable means of control if the surgical platform is subjected to changes, i.e. when the thickness of the abdominal wall is increased, thus affecting the inter-magnetic (i.e. in between the external and internal PMs) interaction. The magnetic field coupling between two PMs decays exponentially as the inter-magnetic distance increases. This results in the decrease of transmitted torques across the abdominal wall. The reduction in transmitted torque when intermagnetic distance increases will cause pole slipping as the internal PM rotors will lose the capability to keep up with the external PMs. Apart from that, the internal and external anchoring unit will be decoupled when the inter-magnetic distance overcomes the magnetic coupling force. The detailed control of the PM rotor is presented in [Di Natali et. al., 2015].

2.2 2DoF robotic manipulator

The robotic manipulator, as shown in Fig. 1, is based on the cable-driven mechanism which has been widely used in

the design of surgical robotic instruments, especially for the LESS surgical applications [Kim et. al., 2012], [Abbott et. al., 2007]. Cable-driven design provides advantages, such as actuation simplicity, compliance and miniature in size, which are desirable for surgical tasks that require high dexterity in a confined workspace.

The robotic manipulator is in form of continuum arm and actuated by pulling four wires to produce movement in two DOFs. Kinematics analysis of the continuum arm structure [He et. al., 2013] to determine of the relation between the length of wire, which is pulled, and tip angle and pose is performed.

Pose of robotic manipulator (continuum arm)

The schematic diagram of the manipulator is shown in Fig. 2. Let a be an arbitrary point located at length l along the primary backbone. Assuming the primary backbone has constant curvature gives:

$$\frac{\beta}{l_t} = \frac{\theta}{l} \;\Rightarrow\; \theta = \frac{\beta}{l_t} l \tag{1}$$

where l_t is the full length of the arm, β is the angle of the distal tip relative to the Z axis, l is the length along the primary backbone to point a and θ is the angle at point a. Thus, the position of point a in the bending plane (Frame 1) can be expressed as:

$${}^1r_{oa} = \frac{l}{\theta}\begin{bmatrix} 1-C_\theta \\ 0 \\ S_\theta \end{bmatrix} = \frac{l_t}{\beta}\begin{bmatrix} 1-cos(\frac{\beta}{l_t}l) \\ 0 \\ sin(\frac{\beta}{l_t}l) \end{bmatrix} \tag{2}$$

Now, converting the bending plane to the inertial reference frame gives the position of point a:

$$\begin{aligned} {}^0r_{oa} = {}^0R_1\,{}^1r_{oa} &= \frac{l_t}{\beta}\begin{bmatrix} C_\gamma & -S_\gamma & 0 \\ S_\gamma & C_\gamma & 0 \\ 0 & 0 & 1 \end{bmatrix}\begin{bmatrix} 1-cos(\frac{\beta}{l_t}l) \\ 0 \\ sin(\frac{\beta}{l_t}l) \end{bmatrix} \\ &= \frac{l_t}{\beta}\begin{bmatrix} (1-cos(\frac{\beta}{l_t}l))cos(\gamma) \\ sin(\frac{\beta}{l_t}l)sin(\gamma) \\ sin(\frac{\beta}{l_t}l) \end{bmatrix} \end{aligned} \tag{3}$$

Therefore, any arbitrary point located at distance l along the primary backbone can be found based on the generalised co-ordinates γ and β.

Mapping generalised coordinates to wire displacement

Assuming constant curvature of the arm the following relationship for the wire displacement can be derived:

$$q_i = \beta r cos(\gamma + P_i), \tag{4}$$

where q_i is the displacement of wire i within the arm, r the radial distance between the primary backbone and wire i and P_i the angle between the bending plane and wire i on the face of the arm plate. Therefore, a given pose of the continuum arm defined with the generalised co-ordinates γ and β can be converted to wire displacements q_i.

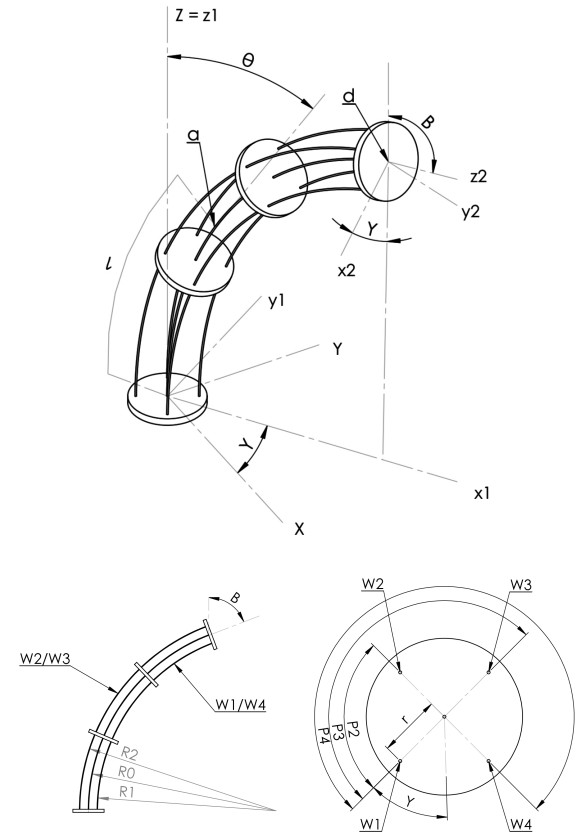

Figure 2: Diagram of continuum arm with coordinate frames and generalised coordinates

Modified wire displacement using straight line segments

The original derivation assumed wires to curve with constant curvature. This assumption is not valid for low number of arm plates and large bending angles. This can be corrected by assuming the wire travels in straight line segments between each arm plate. This leads to the following displacement calculation. Let R_i be the wire arc radius given by:

$$R_i = \frac{l_t}{\beta} - r cos(\gamma + P_i). \tag{5}$$

Let n be the the number of equally spaced arm plates. Now dividing the arc into n segments with each segment subtending an angle given as $\frac{\beta}{n}$. The length of a single segment, C, is given as:

$$C = 2R_i sin(\frac{\beta}{n}). \tag{6}$$

The wire is made up of n segments, thus the displacement of the wire can be calculated as

$$q_i = l_t - nC = l_t - 2n(\frac{l_t}{\beta} - r cos(\gamma + P_i))sin(\frac{\beta}{2n}). \tag{7}$$

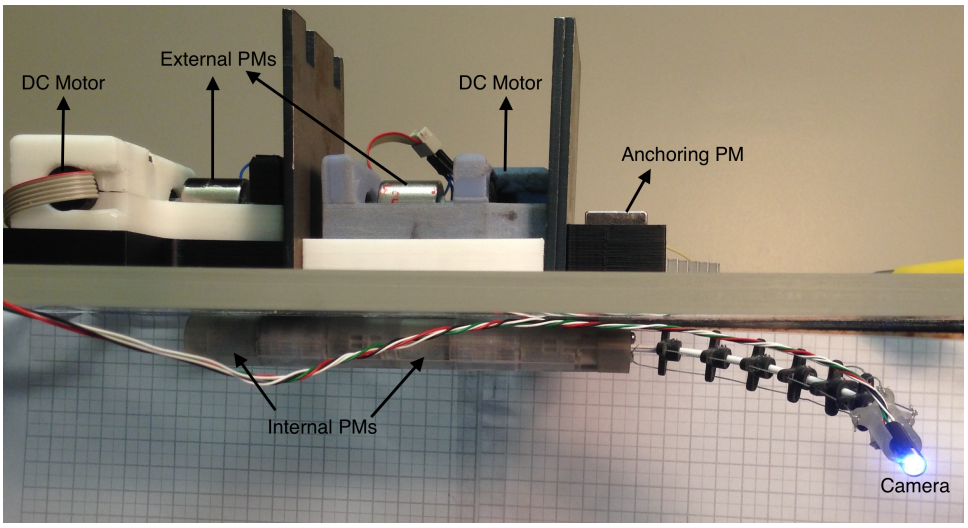

Figure 3: Experimental setup of LMA-based laparoscopic camera

This relation can be used to control the pose of camera attached to the tip of this arm in any desired view angle. In the Section 4 this relation is validated experimentally.

3 Experimental Setup

The experimental setup, as shown in Fig. 3, is composed of an actuation unit, an anchoring unit and a robotic manipulator. The actuation unit consists of DC motors, external and internal PMs, gearboxes and spools. DC motors (1331-006 SR, Faulhaber, Germany) with nominal voltage 6V, were connected with the external PMs by a three-to-one ratio bevel gear set to provide higher torque. Two-channel encoders (IE2-400, Faulhaber, Germany) with 400 lines per revolution were attached to the motors to track the number of motor revolutions. All magnets used in magnetic anchoring and actuation are made of NdFeB, grade N42 (K & J Magnetics). The external and internal PMs are cylindrical. The external PM has diameter and length of 25.4mm and the internal PM has diameter and length of 9.5mm. The external anchoring magnet has dimension: 19mm x 19mm x 9.5mm. The internal anchoring magnet is cylindrical with diameter and length of 9.5mm. The size and strength of the anchoring PMs depends on the weight of the internal unit.

As shown in Fig. 4 The internal actuation unit contains two planetary gearboxes (PM 12, Broadway Gear, Texas) with ratio 121.45:1 and rated efficiency of 73%. Each gearbox has a diameter of 12mm and length of 20.7mm. The spools are directly connected to the output of the gearboxes. Each spool has two groves which allow two wires to be wound in opposite directions; this configuration enables retraction of one wire while releasing the other giving the desired actuation for the continuum arm. The grove has a diameter of 6mm; it also has guides to avoid tangling of the wires.

The robotic manipulator is made of 3D printed wire guides

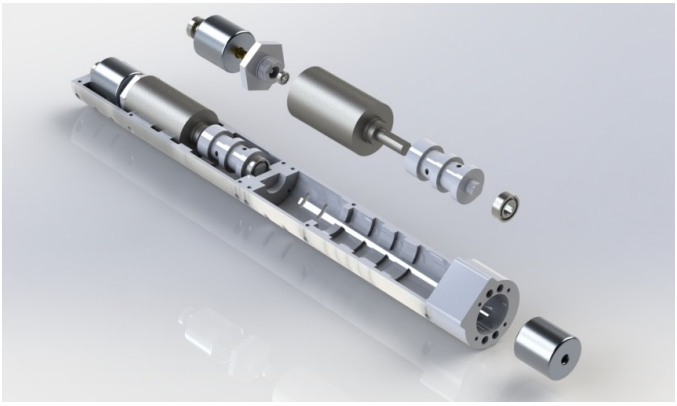

Figure 4: Internal actuation unit

fixed on a backbone. The primary backbone of the robotic manipulator is made of styrene tubing filled with multiple NiTi wires. The super-elastic property of the NiTi wires ensures the backbone stays within the elastic region under high deflection. The wires are made of braided steel to minimise strain under tension while providing flexibility. The tip of the robotic manipulator consist of a camera with light-emitting diodes for illumination.

It was found that the external magnets interfere with each other quite significantly. This issue was addressed by placing 6mm carbon steel plates between each magnet. The plates provide a high permittivity for the magnetic flux thus mitigating the interference. These plates also reduces the interferences of the external anchoring magnets with internal PM rotors.

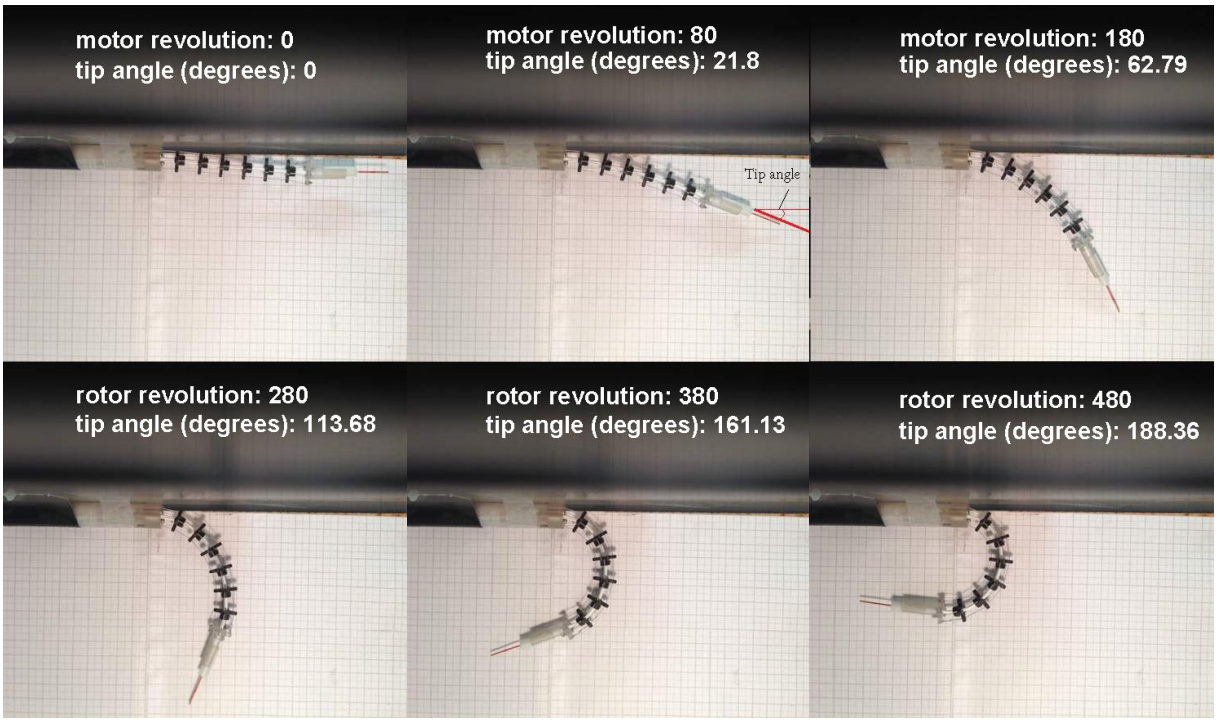

Figure 5: Tip movement of robotic manipulator

4 Experimental Results

An experiment was conducted to obtain the relationship between the number of motor revolutions to the angle of the tip at different distances, h, between the external PM and internal PM. The number of motor revolutions was input at 20 revolutions each step and pictures of the robotic manipulator (continuum arm) were then taken (Fig. 5). For a set distance, h, this procedure was repeated until the tip angle reaches approximately 180°. The tip angles were determined by post processing the images.

As shown in Fig. 6, six sets of data were collected throughout the experiment. These data were plotted against the theoretical model. The experimental data shows a shift on the horizontal axis due to slack in the wire at the start of the test. The gradient of each test followed that of the theoretical model closely thus verifying the theoretical model. The test was repeated with different distance between the external driving PMs and the internal driven PMs, h. The maximum tip angle decreases with larger distance due to the decrease in magnetic attraction between the external and internal PMs. When the tip angle reaches its roll-off angle, the magnets decoupled since the torque required to increase the tip angle is too high. At this point, *pole slipping* occurs. This can be observed in Fig. 6 as the decrease in gradient at the high tip angles although in the medical applications such high tip angles are not required.

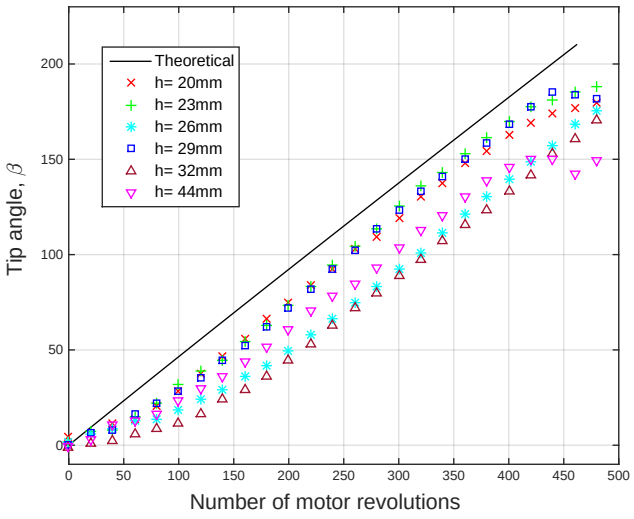

Figure 6: The relation between motor revolutions and tip angle (β) for different distances between external and internal PM (h)

5 Conclusions

An innovative LMA-based surgical camera for laparoscopic surgical approach has been proposed in this paper. The magnetic coupling strategy and cable-driven mechanism design provide the advantages of not requiring onboard actuators and

power units as well as the ability of miniaturising the LMALC design for high degree of intra-abdominal mobility and dexterity. Kinematics of the cable-driven manipulator relating to the motor rotations driven by external magnetic field is presented. Finally, experimental analyses onto the LMALC prototype with varying inter-magnetic distances based on the derived theoretical model were performed. The experimental results demonstrated feasibility and repeatability of the design, which is promising for further studies in the design of controllers.

References

[Di Natali et. al., 2015] Di Natali, Christian, Jacopo Buzzi, Nicol Garbin, Marco Beccani, and Pietro Valdastri. Closed-Loop Control of Local Magnetic Actuation for Robotic Surgical Instruments In *IEEE Transactions on Robotics*, 31(1), pages 43-156, 2015.

[Leung et. al., 2000] Leung Ka Lau, Paul BS Lai, Rocky LK Ho, William CS Meng, Raymond YC Yiu, Janet FY Lee, and Wan Yee Lau. Systemic cytokine response after laparoscopic-assisted resection of rectosigmoid carcinoma: a prospective randomized trial. In *Annals of Surgery*, 231(4), page 506, 2000.

[Johnson, 1997] Alan Johnson. Laparoscopic surgery. In *The Lancet*, 9052(349), pages 631-635, 1997.

[Carbajo et. al., 1999] Carbajo M. A., JC Martn Del Olmo, J. I. Blanco, C. De la Cuesta, M. Toledano, F. Martin, C. Vaquero, and L. Inglada. Laparoscopic treatment vs open surgery in the solution of major incisional and abdominal wall hernias with mesh. In *Surgical Endoscopy*, 13(3), pages 250-252, 1999.

[Romanelli et. al., 2009] Romanelli John R., and David B. Earle. Single-port laparoscopic surgery: an overview. In *Surgical Endoscopy*, 23(7), pages 1419-1427, 2009.

[Tsimoyiannis et. al., 2010] Tsimoyiannis Evangelos C., Konstantinos E. Tsimogiannis, George Pappas-Gogos, Charalampos Farantos, Nikolaos Benetatos, Paraskevi Mavridou, and Adamantia Manataki. Different pain scores in single transumbilical incision laparoscopic cholecystectomy versus classic laparoscopic cholecystectomy: a randomized controlled trial. In *Surgical Endoscopy*, 24(8), pages 1842-1848, 2010.

[Lai et. al., 2000] Lai Fuji, and Robert D. Howe. Evaluating control modes for constrained robotic surgery. In *Proceedings of the International Conference on Robotics and Automation (ICRA)*, 1, pages 603-609, 2000.

[Park et. al., 2007] Park Sangtae, Richard A. Bergs, Robert Eberhart, Linda Baker, Raul Fernandez, and Jeffrey A. Cadeddu. Trocar-less instrumentation for laparoscopy: magnetic positioning of intra-abdominal camera and retractor. In *Annals of Surgery*, 245(3), page 379, 2007.

[Zeltser et. al., 2007] Zeltser Ilia S., Richard Bergs, Raul Fernandez, Linda Baker, Robert Eberhart, and Jeffrey A. Cadeddu. Single trocar laparoscopic nephrectomy using magnetic anchoring and guidance system in the porcine model. In *The Journal of Urology*, 178(1), pages 288-291, 2007.

[Cadeddu et. al., 2009] Cadeddu Jeffrey, Raul Fernandez, Mihir Desai, Richard Bergs, Chad Tracy, Shou-Jiang Tang, Prashanth Rao, Mahesh Desai, and Daniel Scott. Novel magnetically guided intra-abdominal camera to facilitate laparoendoscopic single-site surgery: initial human experience. In *Surgical Endoscopy*, 23(8), pages 1894-1899, 2009.

[Hu et. al., 2009] Hu Tie, Peter K. Allen, Nancy J. Hogle, and Dennis L. Fowler. Insertable surgical imaging device with pan, tilt, zoom, and lighting. In *The International Journal of Robotics Research*, 28(10), pages 1373-1386, 2009.

[Terry et. al., 20012] Terry Benjamin S., Zachary C. Mills, Jonathan Schoen, and Mark E. Rentschler. Single-port access surgery with a novel magnet camera system. In *IEEE Transactions on Biomedical Engineering*, 59(4), pages 1187-1193, 2012.

[Oleynikov, 2008] Dmitry Oleynikov. Robotic surgery. In *Surgical Clinics of North America*, 88(5), pages 1121-1130, 2008.

[Simi et. al., 2013] Massimiliano Simi, Michele Silvestri, Carmela Cavallotti, Monica Vatteroni, Pietro Valdastri, Arianna Menciassi, and Paolo Dario. Magnetically activated stereoscopic vision system for laparoendoscopic single-site surgery. In *IEEE/ASME Transactions on Mechatronics*, 18(3), pages 1140-1151, 2013.

[Di Natali et. al., 2013] Christian Di Natali, Alireza Mohammadi, Denny Oetomo, and Pietro Valdastri. Surgical Robotic Manipulator Based on Local Magnetic Actuation. In *Journal of Medical Devices*, 9(3), page 030936, 2013.

[Kim et. al., 2012] Kim, Chul Sung, Chang-Woo Park, Bong-Seok Kim, Jae-Bok Song, and Jung-Hoon Hwang. Design of robotic surgical instrument for minimally invasive surgical robot system. In *Proceedings of International Conference on Control, Automation and Systems (ICCAS)*, pages 1720-1723, 2012.

[Abbott et. al., 2007] Abbott, Daniel J., Chris Becke, Richard Rothstein, and William J. Peine. Design of an endoluminal NOTES robotic system. In *Proceedings of IEEE/RSJ International Conference on Intelligent Robots and Systems (IROS)*, pages 410-416, 2007.

[He et. al., 2013] He, Bin, Zhipeng Wang, Qiang Li, Hong Xie, and Runjie Shen. An analytic method for the kinematics and dynamics of a multiple-backbone continuum robot. In *International Journal of Advanced Robotic Systems*, 10(84), pages 1-13, 2013.